Numerical study on the incompressible Euler equations as a Hamiltonian system : sectional curvature and Jacobi field

K. Ohkitani

Department of Applied Mathematics,

The University of Sheffield,

Hicks Building, Hounsfield Road,

Sheffield S3 7RH, U.K.

(Dated: March 23, 2010)

Abstract

We study some of the key quantities arising in the Arnold's theory (1966) of the incompressible Euler equations both in two and three dimensions. The sectional curvatures for the Taylor-Green vortex and the ABC flow initial conditions are calculated exactly in three dimensions. We trace the time evolution of the Jacobi fields by direct numerical simulations and, in particular, see how the sectional curvatures get more and more negative in time. The spatial structure of the Jacobi fields is compared with the vorticity fields by visualizations. The Jacobi fields are found to grow exponentially in time for the flows with negative sectional curvatures.

In two dimensions, a family of initial data proposed by Arnold (1966) is considered. The sectional curvature is observed to change its sign quickly even if it starts from a positive value. The Jacobi field is shown to be correlated with the passive scalar gradient in spatial structure.

On the basis of Rouchon's physical-space based expression for the sectional curvature (1984), the origin of negative curvature is investigated. It is found that a 'potential' $\alpha_{\boldsymbol{\xi}}$ appearing in the definition of covariant time derivative plays an important role, in that a rapid growth in its gradient makes a major contribution to the negative curvature.

PACS numbers: 47.10.Df, 47.20.Cq

I. INTRODUCTION

A variational formulation for the Euler equations has been developed[1] and has been proposed to study instability of fluid motion in the Lagrangian sense. This is done by regarding the Euler equations as an infinite-dimensional Hamiltonian system and hence the theory is differential geometric in nature.

In this framework, a geodesic curve on a manifold of volume-preserving flow maps corresponds to each realization of the 3D Euler equations. Deviations of the geodesic curves describe possible instability of fluids and specifically a sectional curvature associated with the geodesic has been proposed to measure the Lagrangian stability of a flow field. Roughly speaking, if the curvature is negative we expect instability with an exponential growth in the Jacobi field and if it's non-negative neutral stability[1–3].

The Hamiltonian method is believed to be the most fundamental formulation of inviscid fluid dynamics, where the Jacobi field and the sectional curvature play an important role. But apparently no studies have looked at them by direct numerical simulations of the Euler equations. One reason is that practical calculations in wavenumber space, on which the evaluations of the sectional curvatures for steady flows are based, are not very useful for the implementations of direct numerical simulations. Here we use an equivalent formulation of splitting the Jacobi's equation into two first-order equations in physical space.

A simple example of a steady solution the 2D Euler equations was used to show that sectional curvature takes negative values for some cross sections[1]. This computation was done by working with Fourier series expansions. Later, this result was extended to three dimensions where the ABC flow is shown to have a negative sectional curvature, again using Fourier series[4]. See also a generalization to the magnetohydrodynamic case[5]. We also note that a local existence theorem of the 3D Euler equations has been obtained on the basis of a differential geometric approach[6,7].

A recent progress on mathematical side is about the relationship between Lagrangian and Eulerian stability analyses[8–10]. One objective is to show that these two kinds of stability criteria are equivalent. A result in this direction states that, for steady two-dimensional flows without stagnation points, if the Eulerian perturbations (measured by $\boldsymbol{f}$ below) are bounded, then no Jacobi field ($\boldsymbol{\xi}$ below) can grow faster than quadratically in time.[10]

The Arnold's formulation was recast by Rouchon[11] in a traditional language that fluid

dynamicists (including the present author) can comprehend with ease. This formulation is based in physical space.

It gives, in particular, a useful integral formula for the sectional curvature in *physical space*, (see (13) below). On this basis, it was established that for every Euler flow, except for pure rotation, there exits at least a direction along which the curvature takes a negative value. This suggests that every Euler flow has at least one unstable direction (associated with the velocity field and a Jacobi field) at any time. This result has been extended to the case of compressible fluids[12].

In spite of these advances, with purely analytical methods the evaluation of the sectional curvatures have been restricted to simple cases of steady flows. It has not been tested to non-stationary flows which may be more relevant, say, to the problem of the onset of turbulence.

The purpose of this paper is three-fold. First, we present exact evaluations of the sectional curvatures for the Taylor-Green vortex and the ABC flow for a number of cross sections by using Rouchon's formula for them. It has turned out that some of them are zero and others are negative. Also, this confirms the equivalence of the two kinds of calculations of the sectional curvature (for the cases of the ABC flow and Arnold's 2D example); the traditional one in Fourier series and the new one using Rouchon's formula. Second, we present the numerical results on the time evolution of the Jacobi fields for that kind of initial conditions. In particular, we show how the sectional curvature gets more and more negative in time. Apparently, no attempts have been reported to follow the Jacobi field and the sectional curvature of fluid dynamical equations by direct numerical simulations. We also compare the structure of the Jacobi field with the vorticity by visualizations. Third, we examine 2D problems in some details by similar methods.

We also note that for the case of ordinary differential equations in classical mechanics of particles, there are some challenging and interesting results which estimate curvature statistics by numerical methods[13–15]. For applications of the methods of Hamiltonian mechanics to fluid dynamics, see e.g. Ref. 6 or Refs. 16-18. For a primitive attempt of geometrization of fluid mechanics, Refs. 19, 20 may be of historical interest.

The rest of the paper is organized as follows. In Section II, we present the mathematical formulation and recapitulate Rouchon's formula and inequalities. In section III, the results of 3D computations are given. Examples of analytical evaluations of the sectional curvatures

for some initial data and numerical results on the time evolution thereof are presented. In Section IV, the case 2D Euler equations is described. Finally, summary and discussion are given in Section V.

II. FUNDAMENTALS

A. Mathematical formulation

We briefly describe Arnold's theory following Rouchon's exposition. We recapitulate the results only and send the interested readers to Ref. 11 for derivations.

We consider the 3D incompressible Euler equations:

$$\frac{D\boldsymbol{u}}{Dt} = -\nabla p, \quad \nabla \cdot \boldsymbol{u} = 0, \tag{1}$$

where $\boldsymbol{u}$ denotes the velocity field and p the pressure. By the vorticity equations

$$\frac{D\boldsymbol{\omega}}{Dt} = (\boldsymbol{\omega} \cdot \nabla)\boldsymbol{u} \tag{2}$$

and by

$$\frac{D^2\boldsymbol{\omega}}{Dt^2} = -\boldsymbol{P} \cdot \boldsymbol{\omega} \tag{3}$$

we have

$$\begin{aligned} \frac{D^2}{Dt^2}\frac{|\boldsymbol{\omega}|^2}{2} &= \left(\frac{D\boldsymbol{\omega}}{Dt}\right)^2 - \boldsymbol{\omega} \cdot \boldsymbol{P} \cdot \boldsymbol{\omega}, \\ &= (\boldsymbol{\omega} \cdot \boldsymbol{S})(\boldsymbol{S} \cdot \boldsymbol{\omega}) - \boldsymbol{\omega} \cdot \boldsymbol{P} \cdot \boldsymbol{\omega}, \end{aligned} \tag{4}$$

where $\boldsymbol{P} = \nabla\nabla p$ denotes the Hessian matrix of the pressure and $\boldsymbol{S}$ the rate-of-strain tensor; see, e.g. Ref. 21.

We recall that in differential geometry, the concept of covariant derivative plays an important role, which is close to, but slightly different from Lagrangian derivative. Actually, covariant derivative is just a solenoidal projection of Lagrangian derivative[22]. More precisely, we have for any function $\boldsymbol{F}(\boldsymbol{x}, t)$

$$\frac{\nabla}{\partial t}\boldsymbol{F}(\boldsymbol{x}, t) \equiv \frac{D\boldsymbol{F}(\boldsymbol{x}, t)}{Dt} + \nabla\alpha_{\boldsymbol{F}}, \tag{5}$$

where $\alpha_{\boldsymbol{F}}$ is there to ensure $\nabla \cdot \frac{\nabla}{\partial t}\boldsymbol{F}(\boldsymbol{x}, t) = 0$. We recall the Jacobi's equation in differential geometry[23], which is second-order in t

$$\frac{\nabla^2}{\partial t^2}\boldsymbol{\xi} = -\boldsymbol{R}(\boldsymbol{\xi}, \boldsymbol{u}) \cdot \boldsymbol{u}. \tag{6}$$

Here $\boldsymbol{R}(\boldsymbol{\xi}, \boldsymbol{u})$ is a curvature tensor and $\boldsymbol{\xi}$ is the Jacobi field along $\boldsymbol{x}$, a more precise meaning of which will be given below. (Note that $\boldsymbol{u} = \frac{D\boldsymbol{x}}{Dt} = \frac{\nabla}{\partial t}\boldsymbol{x}$.) Its direct consequence is

$$\frac{\nabla^2}{\partial t^2}\frac{|\boldsymbol{\xi}|^2}{2} = \left(\frac{\nabla}{\partial t}\boldsymbol{\xi}\right)^2 - \boldsymbol{\xi}\cdot\boldsymbol{R}(\boldsymbol{\xi},\boldsymbol{u})\cdot\boldsymbol{u}. \tag{7}$$

Also, the geodesic equation may be written as

$$\frac{\nabla}{\partial t}\boldsymbol{u} = 0.$$

It may be of interest to note a formal correspondence $\boldsymbol{\omega} \leftrightarrow \boldsymbol{\xi}$ and $\boldsymbol{P}\cdot\boldsymbol{\omega} \leftrightarrow \boldsymbol{R}(\boldsymbol{\xi},\boldsymbol{u})\cdot\boldsymbol{u}$ *provided* we identify $\frac{D}{Dt} \leftrightarrow \frac{\nabla}{\partial t}$. However, the difference between the Lagrangian and covariant derivatives is important, as it gives rise to a major contribution to the negative curvature: the second term on the RHS of (13) below. At any rate, that the pressure Hessian is closely related to the sectional curvature.

The differential geometric approach studies stability of fluid particle trajectories. Hence we need the 3D Euler equations together with the equation for particle trajectories

$$\begin{cases} \dfrac{\partial \boldsymbol{u}}{\partial t} + \boldsymbol{u}\cdot\nabla\boldsymbol{u} = -\nabla p, \\ \dfrac{D\boldsymbol{x}(\boldsymbol{a},t)}{Dt} = \boldsymbol{u}(\boldsymbol{x}(\boldsymbol{a},t),t),\ \boldsymbol{x}(\boldsymbol{a},0) = \boldsymbol{a}. \end{cases} \tag{8}$$

We consider small perturbations on the spatial position and the velocity of a fluid element $\boldsymbol{a}$. These perturbations are characterized by a parameter s, where $s = 0$ corresponds to an unperturbed state. We then write $\boldsymbol{x}(\boldsymbol{a}, t; s)$ for the position of perturbed paths at time t. We consider a perturbation (or variation) $\boldsymbol{\xi}$ of the spatial position and a perturbation $\boldsymbol{f}$ of the velocity. We may define those by

$$\boldsymbol{f}(\boldsymbol{x},t) \equiv \frac{\partial}{\partial s}\boldsymbol{u}(\boldsymbol{a},t;s)\bigg|_{s=0} = \delta\boldsymbol{u},\ \ \boldsymbol{\xi}(\boldsymbol{x},t) \equiv \frac{\partial}{\partial s}\boldsymbol{x}(\boldsymbol{a},t;s)\bigg|_{s=0}.$$

The variable $\boldsymbol{\xi}$ is called the Jacobi field[24].

By linearizing both equations in (8) using a chain rule, we obtain the following set of equations in place of the Jacobi field[11]

$$\begin{cases} \dfrac{D\boldsymbol{\xi}}{Dt} = (\boldsymbol{\xi}\cdot\nabla)\boldsymbol{u} + \boldsymbol{f},\ \ \nabla\cdot\boldsymbol{\xi} = 0, \\ \dfrac{D\boldsymbol{f}}{Dt} = -(\boldsymbol{f}\cdot\nabla)\boldsymbol{u} - \nabla q,\ \ \nabla\cdot\boldsymbol{f} = 0, \end{cases} \tag{9}$$

the latter of which is nothing but the linearized Euler equations. Here q denotes another potential. The former reduces to the vorticity equations if $\boldsymbol{f}$ is neglected.

If we consider

$$\frac{\nabla}{\partial t}\boldsymbol{\xi}(\boldsymbol{x},t) \equiv \frac{D\boldsymbol{\xi}(\boldsymbol{x},t)}{Dt} + \nabla\alpha_{\boldsymbol{\xi}}$$

by using (5), we find $\nabla\cdot((\boldsymbol{\xi}\cdot\nabla)\boldsymbol{u}) + \triangle\alpha_{\boldsymbol{\xi}} = 0$, or equivalently,

$$\nabla\cdot((\boldsymbol{u}\cdot\nabla)\boldsymbol{\xi}) + \triangle\alpha_{\boldsymbol{\xi}} = 0.$$

for the equation for a 'potential' $\alpha_{\boldsymbol{\xi}}$.

Noting

$$\frac{D}{Dt}(\boldsymbol{\xi}\cdot\nabla) = \boldsymbol{f}\cdot\nabla,$$

we have

$$\frac{D^2\boldsymbol{\xi}}{Dt^2} = -\boldsymbol{P}\cdot\boldsymbol{\xi} - \nabla q. \tag{10}$$

We use the definition of covariant derivative twice to obtain the equations for the Jacobi field

$$\frac{\nabla^2}{\partial t^2}\boldsymbol{\xi} + \boldsymbol{A}_{\boldsymbol{u}}(\boldsymbol{\xi}) = 0, \tag{11}$$

where

$$\boldsymbol{A}_{\boldsymbol{u}}(\boldsymbol{\xi}) \equiv \boldsymbol{P}\cdot\boldsymbol{\xi} - (\boldsymbol{u}\cdot\nabla)\nabla\alpha_{\boldsymbol{\xi}} + \nabla\gamma. \tag{12}$$

We have the following symmetry

$$\langle\boldsymbol{\xi}_1, \boldsymbol{A}_{\boldsymbol{u}}(\boldsymbol{\xi}_2)\rangle = \langle\boldsymbol{\xi}_2, \boldsymbol{A}_{\boldsymbol{u}}(\boldsymbol{\xi}_1)\rangle = \langle\boldsymbol{\xi}_1\cdot\boldsymbol{P}\cdot\boldsymbol{\xi}_2 - \nabla\alpha_{\boldsymbol{\xi}_1}\cdot\nabla\alpha_{\boldsymbol{\xi}_2}\rangle,$$

which follows from an identity

$$\left\langle\frac{\nabla}{\partial t}\boldsymbol{\xi}_1\cdot\nabla\alpha_{\boldsymbol{\xi}_2}\right\rangle = 0.$$

In this paper the brackets denote a spatial average in a periodic domain, that is, $\langle\ \ \rangle = \frac{1}{V}\int\boldsymbol{dx}, V = (2\pi)^3$ in three dimensions. Setting

$$2U_{\boldsymbol{u}}(\boldsymbol{\xi}) = \left\langle\boldsymbol{\xi}\cdot\boldsymbol{P}\cdot\boldsymbol{\xi} - |\nabla\alpha_{\boldsymbol{\xi}}|^2\right\rangle, \tag{13}$$

we finally find[25]

$$\frac{1}{V}\frac{\nabla^2}{\partial t^2}\boldsymbol{\xi} = -\frac{\delta U_{\boldsymbol{u}}(\boldsymbol{\xi})}{\delta\boldsymbol{\xi}},$$

where $\frac{\delta}{\delta\boldsymbol{\xi}}$ denotes a functional derivative. We define the sectional curvature in the directions of $\boldsymbol{u}$ and $\boldsymbol{\xi}$ by

$$C(\boldsymbol{u},\boldsymbol{\xi}) = \frac{2U_{\boldsymbol{u}}(\boldsymbol{\xi})}{\langle|\boldsymbol{u}|^2\rangle\langle|\boldsymbol{\xi}|^2\rangle - \langle(\boldsymbol{u}\cdot\boldsymbol{\xi})^2\rangle},$$

or $K(\boldsymbol{u},\boldsymbol{\xi}) = \frac{1}{V}C(\boldsymbol{u},\boldsymbol{\xi})$, after normalization. Note that $2U_{\boldsymbol{u}}(\boldsymbol{\xi}) = \langle\boldsymbol{\xi}\cdot\boldsymbol{R}(\boldsymbol{\xi},\boldsymbol{u})\cdot\boldsymbol{u}\rangle$.

B. Bounds for the sectional curvature

The matrix $\boldsymbol{M} \equiv \boldsymbol{P} - (\nabla \boldsymbol{u})^T \nabla \boldsymbol{u}$ introduced in Ref. 11 has a dimension of $[\boldsymbol{M}] = \text{time}^{-2}$ and was interpreted as setting the time scale of particle dispersion. Using this matrix, the following inequalities have been established[11]

$$2U_{\boldsymbol{u}}(\boldsymbol{\xi}^{\perp}) \geq \frac{1}{V} \int \boldsymbol{\xi}^{\perp} \cdot \boldsymbol{M} \cdot \boldsymbol{\xi}^{\perp} d\boldsymbol{x}, \tag{14}$$

$$\frac{1}{3V} \min_{\boldsymbol{x}} \text{tr}(\boldsymbol{M}(\boldsymbol{x}, t)) \geq \min_{\|\boldsymbol{\xi}\|=1} 2U_{\boldsymbol{u}}(\boldsymbol{\xi}) \geq \frac{1}{V} \min_{\boldsymbol{x}} \lambda_{\min}(\boldsymbol{x}, t). \tag{15}$$

where $\lambda_{\min}$ is the smallest of the eigenvalues of $\boldsymbol{M}$.

The proof uses an elementary identity

$$\text{tr}(\boldsymbol{M}(\boldsymbol{x}, t)) = \triangle p - (\partial_i u_j)(\partial_i u_j) = -\text{tr}(\boldsymbol{S} \cdot \boldsymbol{S}) \leq 0.$$

More importantly, the upper bound in (15) states that unless $\boldsymbol{S} \equiv 0$, we can always find negative sectional curvature for some cross sections. This may be interpreted as the existence of unstable directions for Euler flows at any time. We note that the analysis is slightly dynamical as it involves the pressure term.

However, it tells nothing about how such directions associated with negative curvatures relate to the dynamics of the Euler equations. For example, it is not clear whether the Jacobi fields follow the unstable directions in time to make the associated sectional even more negative or not. Hence, some numerical approach is required. We also study a property of the matrix $\boldsymbol{M}$ numerically in subsection IV.C.

III. 3D COMPUTATIONAL RESULTS

A. Analytic evaluation of sectional curvature

First, we check with the evaluation of the sectional curvature of the ABC flow in the directions of

$$\boldsymbol{u} = \begin{pmatrix} A\sin z + C\cos y \\ B\sin x + A\cos z \\ C\sin y + B\cos x \end{pmatrix} \text{ and } \boldsymbol{\xi} = \begin{pmatrix} a\sin z + c\cos y \\ b\sin x + a\cos z \\ c\sin y + b\cos x \end{pmatrix}.$$

By solving two equations

$$\triangle p = -\nabla \cdot ((\boldsymbol{u} \cdot \nabla)\boldsymbol{u}), \tag{16}$$

$$\triangle \alpha_{\boldsymbol{\xi}} = -\nabla \cdot ((\boldsymbol{\xi} \cdot \nabla)\boldsymbol{u}) \tag{17}$$

we obtain two potentials (or, pressures-like quantities) p and $\alpha_{\boldsymbol{\xi}}$. Plugging them into (13), we find

$$2U_{\boldsymbol{u}}(\boldsymbol{\xi}) = -\frac{1}{8}\left((aB - bA)^2 + (bC - cB)^2 + (cA - aC)^2\right) \leq 0.$$

(In practice, we may have recourse to symbolic manipulations to work it out. A sample script may be obtained from `http://www.koji-ohkitani.staff.shef.ac.uk/papers`.) This completely agrees with the result using Fourier series[4], where a more general case was treated. It shows that the curvature is negative-definite and $U_{\boldsymbol{u}}(\boldsymbol{\xi})$ is zero if and only if (a, b, c) and (A, B, C) are parallel.

Next, we consider the initial condition of the Taylor-Green vortex

$$\boldsymbol{u} = \begin{pmatrix} A\cos x \sin y \sin z \\ B \sin x \cos y \sin z \\ C \sin x \sin y \cos z \end{pmatrix}, \text{ with } A + B + C = 0$$

We consider two kinds of initial conditions of the Jacobi fields.

Case 1 (velocity type)

$$\boldsymbol{\xi} = \begin{pmatrix} a\cos x \sin y \sin z \\ b \sin x \cos y \sin z \\ c \sin x \sin y \cos z \end{pmatrix}, \text{ with } a + b + c = 0$$

Again using symbolic manipulations, the result turns out to be simply

$$2U_{\boldsymbol{u}}(\boldsymbol{\xi}) \equiv 0,$$

irrespective of the choice of A, B, C and a, b, c. We knew that it vanishes for $A = a,\ B = b,\ C = c$, because the Jacobi fields in the direction of the velocity is irrelevant[25]. However, the vanishing of the curvature in more general cases $(A, B, C) \neq (a, b, c)$ is non-trivial.

Second, we choose the Jacobi field to have a similar functional dependence as the vorticity (with lower case amplitudes).

Case 2 (vorticity type)

We consider

$$\boldsymbol{\xi} = \begin{pmatrix} (c - b)\sin x \cos y \cos z \\ (a - c)\cos x \sin y \cos z \\ (b - a)\cos x \cos y \sin z \end{pmatrix}.$$

By the same procedure, we find

$$2U_{\boldsymbol{u}}(\boldsymbol{\xi}) = -\frac{3}{128}\left(a^2B^2 + b^2A^2 + 2(bA - aB)^2\right.$$

$$\left.+(A+B)^2(a^2+b^2) + (a+b)^2(A^2+B^2)\right) \leq 0$$

In these cases it turns out to be negative-definite, just like the case of ABC flow.

B. Numerical simulation of Jacobi field and sectional curvature

Here we are interested in the time evolution of the sectional curvatures and the Jacobi fields, which have not been reported by numerical simulations. To study this we solve simultaneously the 3D Euler equations together with the Jacobi's equations numerically. That way, we may study how the Jacobi fields evolve in time and compare their behaviors with those of flow fields.

Numerically we employ a standard pseudo-spectral method with 2/3-dealiasing. Typical grid points used are 256^3 and 512^3. For time marching, we use fourth-order Runge-Kutta method with a typical time step $\Delta t = 10^{-3}$. Because we solve the inviscid equations the flows become under-resolved rather quickly. By monitoring the analyticity strip we estimate the computation remains reliable up to about $t = 2$ at 512^3, see Fig.1 and 2 for energy spectra defined by $E(k) \equiv \sum_{k \leq |\boldsymbol{k}| < k+1} |\boldsymbol{u}(\boldsymbol{k})|^2/2$. There are no noticeable differences in the post-processing of the numerical data (e.g. visualizations and correlations) between resolutions. We use mainly the 256^3 data for visualizations.

We treat the Taylor-Green vortex numerically for the two cases.

Case 1

We set $A = a = 1, B = b = -1, C = c = 0$. The Jacobi equation is second-order in time and the (second) initial condition for $\boldsymbol{f}$ is taken as $\boldsymbol{f}(\boldsymbol{x}) = \boldsymbol{\omega}(\boldsymbol{x})$. The initial condition for $\boldsymbol{\xi}$ is similar to the velocity. We show time evolution of (unnormalized) sectional curvature in Fig.3 to show the contributions of two terms we plot $\langle |\nabla \alpha_{\boldsymbol{\xi}}|^2 \rangle$, $\langle \boldsymbol{\xi} \cdot \boldsymbol{P} \cdot \boldsymbol{\xi} \rangle$, and $2U_{\boldsymbol{u}}(\boldsymbol{\xi})$, separately. In this case, the sectional curvature is zero initially but becomes negative under time evolution, primarily because of a rapid growth in $\langle |\nabla \alpha_{\boldsymbol{\xi}}|^2 \rangle$, together with a mild decrease in $\langle \boldsymbol{\xi} \cdot \boldsymbol{P} \cdot \boldsymbol{\xi} \rangle$.

Case 2

We set again $A = a = 1, B = b = -1, C = c = 0$ and take $\boldsymbol{f}(\boldsymbol{x}) = \boldsymbol{\omega}(\boldsymbol{x})$. The initial

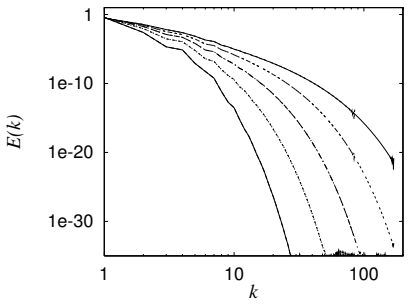

FIG. 1: Time evolution of spectra of energy $E(k)$ for Case 1 at $t = 0.4, 0.8, 1.2, 1.6$ and 2.0 from below. The results from 256^3 and 512^3 computations are overlaid.

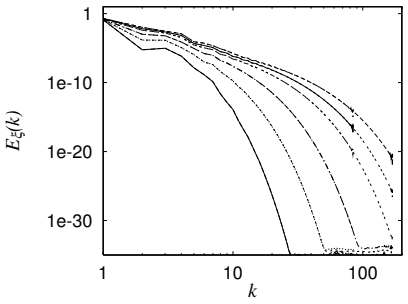

FIG. 2: Time evolution of spectra of Jacaobi field $E_{\boldsymbol{\xi}}(k)$ for Case 1 at $t = 0.4, 0.8, 1.2, 1.6$ and 2.0 from below. The results from 256^3 and 512^3 computations are overlaid.

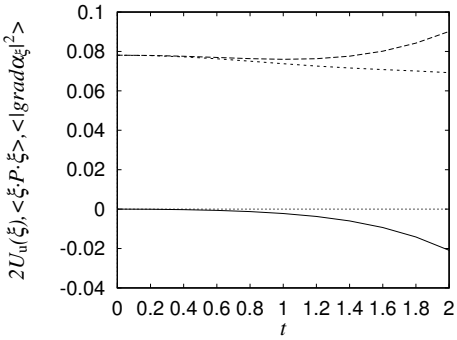

FIG. 3: Time evolution of unnormalized sectional curvature $2U_{\boldsymbol{u}}(\boldsymbol{\xi})$ (solid), $\langle|\nabla\alpha_{\boldsymbol{\xi}}|^2\rangle$ (dashed) and $\langle\boldsymbol{\xi}\cdot\boldsymbol{P}\cdot\boldsymbol{\xi}\rangle$ (short-dashed) for Case 1. The dotted line represents 0.

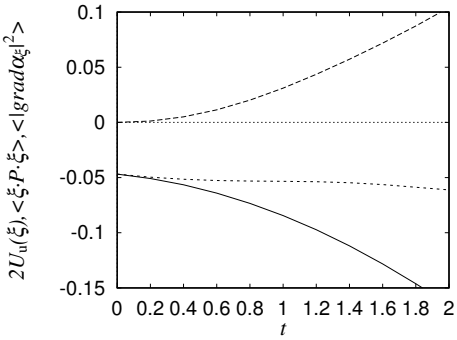

FIG. 4: Time evolution of unnormalized sectional curvature $2U_{\boldsymbol{u}}(\boldsymbol{\xi})$ (solid), $\langle|\nabla\alpha_{\boldsymbol{\xi}}|^2\rangle$ (dashed) and $\langle\boldsymbol{\xi}\cdot\boldsymbol{P}\cdot\boldsymbol{\xi}\rangle$ (short-dashed) for Case 2. The dotted line represents 0.

condition for $\boldsymbol{\xi}$ is similar to the vorticity. In this vorticity-type initial condition for $\boldsymbol{\xi}$, the sectional curvature is already negative at the initial instant of time (Fig.4): $2U_{\boldsymbol{u}}(\boldsymbol{\xi}) = -3/64 = -0.046875$. It becomes more and more negative as time goes on again by a rapid growth of $\langle|\nabla\alpha_{\boldsymbol{\xi}}|^2\rangle$.

C. Spatial structure

We now study spatial structure of the Jacobi field and compare it with the vorticity field. For Case 1 (velocity-type initial condition for $\boldsymbol{\xi}$), we show in Fig.5 and 6 the iso-surface

plots of $|\boldsymbol{\omega}|^2$ and $|\boldsymbol{\xi}|^2$ in a box $[0, \pi/2]^3$. The thresholds are chosen as $|\boldsymbol{\omega}|^2 = \langle|\boldsymbol{\omega}|^2\rangle$ and $|\boldsymbol{\xi}|^2 = \langle|\boldsymbol{\xi}|^2\rangle$. The region with large vorticity has a layer-like structure, which is typical in the early stage evolution of the Euler equations. While these plots suggests that the spatial correlation is growing between vorticity and Jacobi field $\boldsymbol{\xi}$ qualitatively, it is not easy to see whether and how this is taking place. In view of the similarity between the vorticity $\boldsymbol{\omega}$ and the Jacobi field $\boldsymbol{\xi}$ mentioned in Section II.A, it is of interest to check this point quantitatively. We plot in Fig.7 the correlation coefficient $r(\boldsymbol{\omega}, \boldsymbol{\xi})$ between $\boldsymbol{\omega}$ and $\boldsymbol{\xi}$, defined by

$$r(\boldsymbol{\omega}, \boldsymbol{\xi}) = \frac{\langle \boldsymbol{\omega} \cdot \boldsymbol{\xi} \rangle}{\sqrt{\langle|\boldsymbol{\omega}|^2\rangle \, \langle|\boldsymbol{\xi}|^2\rangle}}.$$

It clearly shows that the correlation grows monotonically in time and reaches a value of about 0.5. This gives some support to the formal similarity between the vorticity and the Jacobi field in Section II.A.

For the Case 2, the initially they are perfectly correlated ($\boldsymbol{\omega} = \boldsymbol{\xi}$ at $t = 0$ by initialization). We show in Fig.8 and 9 the iso-surface plots of $|\boldsymbol{\omega}|^2$ and $|\boldsymbol{\xi}|^2$. As far as the time interval covered by the present computations, the spatial structures remain close to each other. In fact, the correlation coefficient stays at a high level throughout the time evolution and is still 0.97 at $t = 2.0$ (figure omitted).

The above results show that the Jacobi field tends to build a strong correlation with the vorticity field and that strong a correlation once developed tends to persist under the time evolution.

IV. 2D COMPUTATIONAL RESULTS

As a counterpart to the vorticity in 3D, in 2D it is the vorticity gradient $\boldsymbol{\chi} = \nabla^\perp \omega$ which becomes large. It satisfies

$$\frac{D\boldsymbol{\chi}}{Dt} = \boldsymbol{\chi} \cdot \nabla \boldsymbol{u},$$

where $\nabla^\perp = (\partial_y, -\partial_x)$. Hence $\boldsymbol{\chi}$ is expected to behave similarly as Jacobi field. The framework of Jacobi's equation itself essentially remains the same as in 3D.

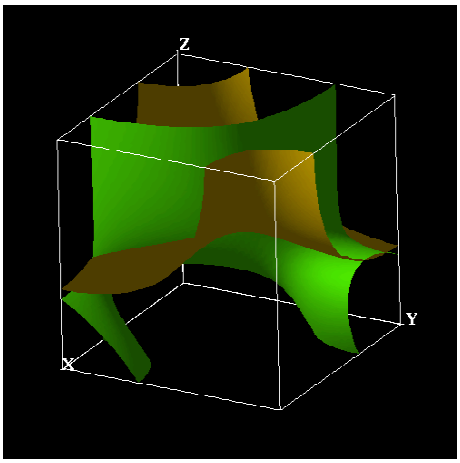

FIG. 5: Iso-vorticity surface of $|\boldsymbol{\xi}|^2$(gray, yellow online) and $|\boldsymbol{\omega}|^2$(dark gray, green online) at $t = 0.4$ for Case 1.

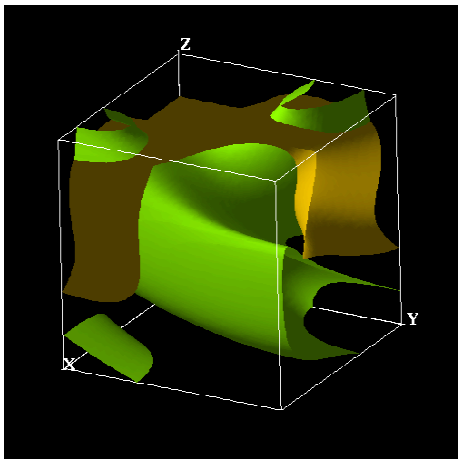

FIG. 6: Iso-vorticity surface of $|\boldsymbol{\xi}|^2$(gray, yellow online) and $|\boldsymbol{\omega}|^2$(dark gray, green online) at $t = 2.0$ for Case 1.

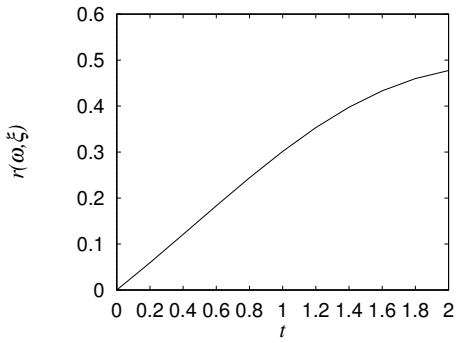

FIG. 7: Time evolution of the correlation coefficient $r(\boldsymbol{\omega}, \boldsymbol{\xi})$ between the vorticity and the Jacobi field.

A. Analytic evaluation of sectional curvature

Using Fourier series some sectional curvatures were evaluated for a class of flows of the 2D Euler equations[1]. It may be illustrative to derive them using (13), which is based in physical space, because it clarifies how the negative curvature shows up. It it noted that this information is not available if we work in Fourier representation.

For a class of flows defined by a stream function $\psi = \cos \boldsymbol{k} \cdot \boldsymbol{x}$, we consider a section of the form $\psi_{\boldsymbol{\xi}} = \cos \boldsymbol{l} \cdot \boldsymbol{x}$, where $\boldsymbol{k} = (k_1, k_2)$, $\boldsymbol{l} = (l_1, l_2)$. The corresponding velocity and

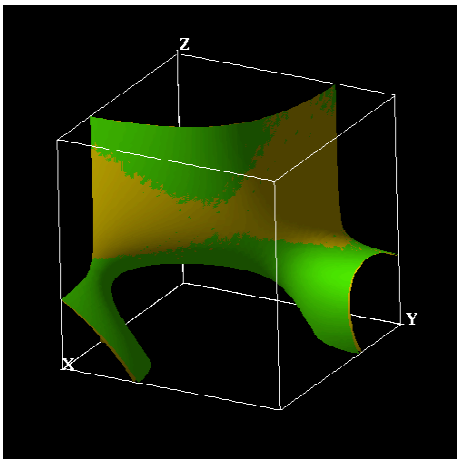

FIG. 8: Iso-vorticity surface of $|\boldsymbol{\xi}|^2$(gray, yellow online) and $|\boldsymbol{\omega}|^2$(dark gray, green online) at $t = 0.4$ for Case 2.

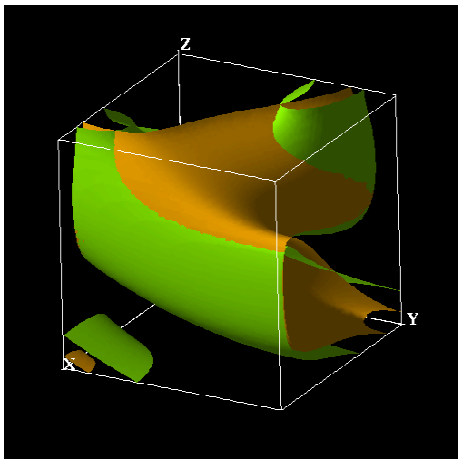

FIG. 9: Iso-vorticity surface of $|\boldsymbol{\xi}|^2$(gray, yellow online) and $|\boldsymbol{\omega}|^2$(dark gray, green online) at $t = 2.0$ for Case 2.

Jacobi fields read

$$\boldsymbol{u} = (-k_2 \sin \boldsymbol{k}\cdot\boldsymbol{x}, k_1 \sin \boldsymbol{k}\cdot\boldsymbol{x}),$$

and

$$\boldsymbol{\xi} = (-l_2 \sin \boldsymbol{l}\cdot\boldsymbol{x}, l_1 \sin \boldsymbol{l}\cdot\boldsymbol{x}),$$

respectively. Then (16) becomes simply

$$\triangle p = 0.$$

Since p is harmonic in the periodic box, it should be a constant and the pressure Hessian vanishes identically; $\boldsymbol{P} = 0$. It should be noted at this stage that the sectional curvature is inevitably negative because of the first term in the integrand in (13) vanishes.

On the other hand, (17) becomes

$$\triangle \alpha_{\boldsymbol{\xi}} = (k_1 l_2 - k_2 l_1)^2 \cos \boldsymbol{k}\cdot\boldsymbol{x} \cos \boldsymbol{l}\cdot\boldsymbol{x},$$

from which it follows that, for $\boldsymbol{k} \neq \pm\boldsymbol{l}$,

$$\alpha_{\boldsymbol{\xi}} = -\frac{(\boldsymbol{k}\times\boldsymbol{l})^2}{2}\left(\frac{\cos(\boldsymbol{k}+\boldsymbol{l})\cdot\boldsymbol{x}}{|\boldsymbol{k}+\boldsymbol{l}|} + \frac{\cos(\boldsymbol{k}-\boldsymbol{l})\cdot\boldsymbol{x}}{|\boldsymbol{k}-\boldsymbol{l}|}\right),$$

and we compute

$$\left\langle |\nabla \alpha_{\boldsymbol{\xi}}|^2 \right\rangle = \frac{|\boldsymbol{k}\times\boldsymbol{l}|^4}{8}\frac{|\boldsymbol{k}+\boldsymbol{l}|^2 + |\boldsymbol{k}-\boldsymbol{l}|^2}{|\boldsymbol{k}+\boldsymbol{l}|^2|\boldsymbol{k}-\boldsymbol{l}|^2} = \frac{|\boldsymbol{k}|^2+|\boldsymbol{l}|^2}{4}\frac{|\boldsymbol{k}\times\boldsymbol{l}|^4}{|\boldsymbol{k}+\boldsymbol{l}|^2|\boldsymbol{k}-\boldsymbol{l}|^2},$$

where $\langle\ \ \rangle = \frac{1}{S}\int\ \boldsymbol{dx},\ S = (2\pi)^2$. Normalizing by $\langle|\boldsymbol{u}|^2\rangle = |\boldsymbol{k}|^2/2$ and $\langle|\boldsymbol{\xi}|^2\rangle = |\boldsymbol{l}|^2/2$ we recover a result[1]

$$C(\boldsymbol{u},\boldsymbol{\xi}) = \frac{2U_{\boldsymbol{u}}(\boldsymbol{\xi})}{S\,\langle|\boldsymbol{u}|^2\rangle\,\langle|\boldsymbol{\xi}|^2\rangle} = -\frac{|\boldsymbol{k}|^2+|\boldsymbol{l}|^2}{4}\sin^2\alpha\sin^2\beta,$$

where α is an angle between $\boldsymbol{k}$ and $\boldsymbol{l}$ and β is an angle between $\boldsymbol{k}+\boldsymbol{l}$ and $\boldsymbol{k}-\boldsymbol{l}$. Note that $\langle\boldsymbol{u}\cdot\boldsymbol{\xi}\rangle = 0$ for $\boldsymbol{k}\neq\boldsymbol{l}$. Note also that the normalized sectional curvature in two dimensions is $K(\boldsymbol{u},\boldsymbol{\xi}) = C(\boldsymbol{u},\boldsymbol{\xi})/S$.

B. Numerical simulation of Jacobi field and sectional curvature

An example of a flow and a Jacobi field which has a positive sectional curvature was given in Ref. 1. The following class of flows was considered there

$$\psi = \epsilon\left(\cos(3px-y)+\cos(3px+2y)\right),$$

$$\psi_{\boldsymbol{\xi}} = \epsilon\left(\cos(px+y)+\cos(px-2y)\right),$$

where p denotes positive integers. It was shown that $K(\boldsymbol{u},\boldsymbol{\xi}) < 0$ at $p = 1$ and $K(\boldsymbol{u},\boldsymbol{\xi}) > 0$ at $p = 2$ and that with $\epsilon = 1$

$$K(\boldsymbol{u},\boldsymbol{\xi}) \to \frac{9}{8\pi^2},\ \text{as}\ p\to\infty.$$

Although straightforward, the evaluation of the sectional curvature for general p is complicated. Using (13) we may work out for $p = 1, 2$ explicitly as follows.

Here we take $\epsilon = 0.01$ for numerical purposes. At $p = 1$, we find

$$C(\boldsymbol{u},\boldsymbol{\xi}) = -\frac{5913}{100}\epsilon^4 = -\frac{5913}{1000000} = -0.005913$$

which is negative. At $p = 2$, we have

$$C(\boldsymbol{u},\boldsymbol{\xi}) = \frac{432612}{6205}\epsilon^4 = \frac{108153}{15512500} \approx 0.006971,$$

which has changed its sign as stated in Ref. 1.

We have performed numerical simulations of the 2D Euler equations with the Jacobi field equations for the two cases of the initial conditions Case 1 ($p = 1$) and Case 2 ($p = 2$) using 2/3-dealised pseudo-spectral computations on 1024^2 grid points.

First we check the enstrophy spectra $Q(k) \equiv \sum_{k \le |\boldsymbol{k}| < k+1} |\omega(\boldsymbol{k})|^2/2$ for Case 1 and Case 2 in Fig.10 and 11, to confirm numerical accuracy. We observe wild fluctuations because of higher harmonics of order p at $t = 0$. This is a typical phenomenon where we have interference of near-singular structures in the domain[26].

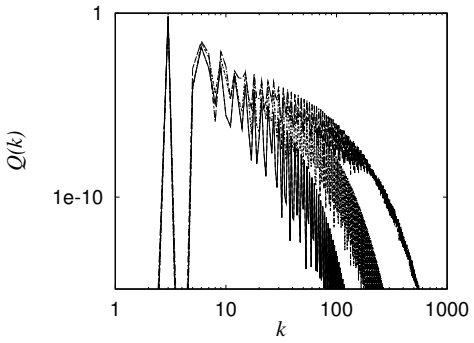

FIG. 10: Time evolution of spectra of enstrophy $Q(k)$ for Case 1 at $t = 2, 3$ and 4.

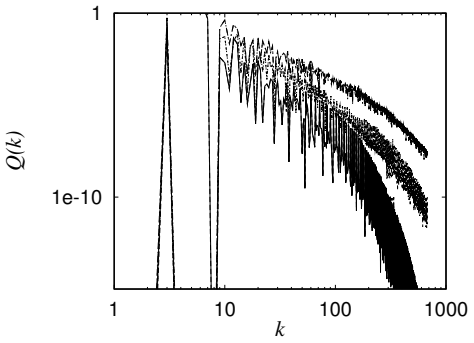

FIG. 11: Time evolution of spectra of enstrophy $Q(k)$ for Case 2 at $t = 1.5, 2$ and 2.5.

We begin considering Case 1. In Fig.12 we show the time evolution of vorticity contours. Initially there are 6 vortices in a period in the x-direction and the early stage evolution proceeds rather slowly. Between $t = 2.0$ and $t = 3.0$ compression and extension of these vortices become noticeable in a spatially alternating manner. In Fig.13 we show the time evolution of the Jacobi field in its 'stream function' form. At $t = 3.0$ or later, we observe large values of the Jacobi field in the regions with mild vorticity gradient, but not with the steepest one. We next consider the integrand of the sectional curvature in Fig.14. In the early stage of its development, say $t \le 2.0$, its signature is neither clearly correlated with vorticity gradient nor with the Jacobi field. But later at $t \ge 3.0$ it is strongly correlated with them. The numerical results show that large values of the Jacobi field and large (negative) values of the sectional curvature are highly correlated, and is also associated with mild vorticity gradient.

We now consider the time evolution of norms in Fig.15, where we confirm the vorticity gradient and the Jacobi field grow exponentially in time. In Fig.16, the time evolution of the sectional curvature is shown, together with its breakdown, that is, separate contributions from each term in (9). We observe that the sectional curvature becomes even more negative as time goes on and that this mainly comes from a rapid growth in the gradient of $\nabla \alpha_{\boldsymbol{\xi}}$.

Now we consider Case 2. The time evolution of contours of vorticity and those of the

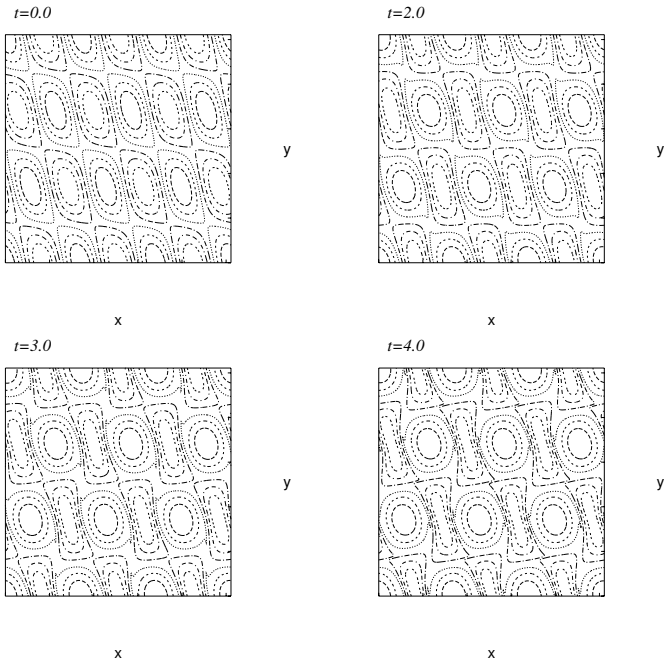

FIG. 12: Time evolution of contours of vorticity ω for Case 1 in $[0, 2\pi]^2$. Five equally spaced levels are used between the maximum and the minimum.

Jacobi field is shown in Fig.17 and 18, respectively. In this case, the large values of the Jacobi field coincide with steep gradient of vorticity at late times. It should be noted that the patterns of $\psi_{\boldsymbol{\xi}}$ at, say, $t = 2.5$ is markedly different from that of $t = 0$. In Fig.19, we show the integrand of the sectional curvature, where we confirm that it take large values in those regions with steep vorticity gradient.

The time evolution of norms of vorticity gradient and Jacobi field has been examined. After $t = 2$ they grow exponentially in time (not shown). As seen in Fig.18, this corresponds to the time for $\psi_{\boldsymbol{\xi}}$ to settle in the final pattern. The time evolution of the sectional curvature is also studied. In Fig.20 a close-up view is given where the curvature changes its sign around $t = 0.8$. No special event has been identified in the Jacobi field in physical space at that time. The sectional curvature takes a large negative value (about -250 at $t = 3.0$) in the late stage even it starts from a small positive value.

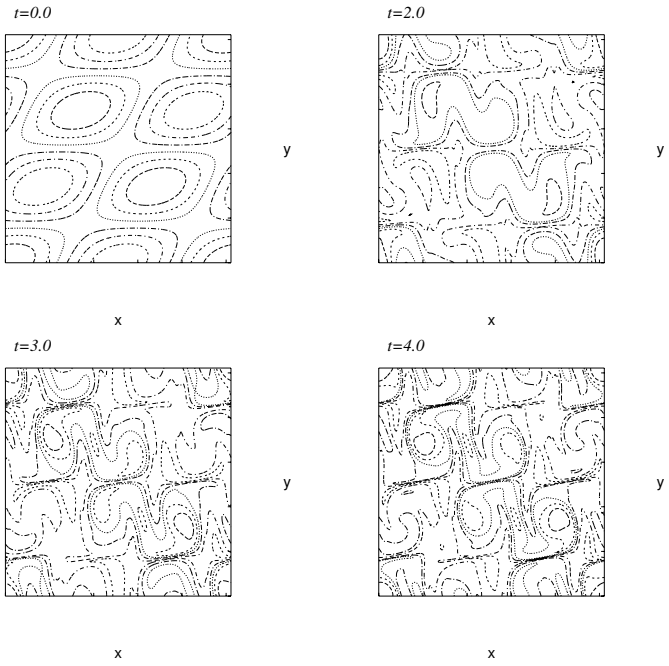

FIG. 13: Time evolution of contours of the Jacobi field $\psi_{\boldsymbol{\xi}}$ for Case 1. Plotted similarly as in Fig.12.

C. Comparison of Jacobi and passive scalar fields

Here we examine the correlation coefficient $r(\omega, \psi_{\boldsymbol{\xi}})$ between the vorticity and the Jacobi fields and the correlation coefficient $r(\nabla\omega, \nabla\psi_{\boldsymbol{\xi}})$ and between their gradients. They are defined respectively by

$$r(\omega, \psi_{\boldsymbol{\xi}}) = \frac{\langle \omega\psi_{\boldsymbol{\xi}} \rangle}{\sqrt{\langle \omega^2 \rangle \langle (\psi_{\boldsymbol{\xi}})^2 \rangle}},\ r(\nabla\omega, \nabla\psi_{\boldsymbol{\xi}}) = \frac{\langle \nabla\omega \cdot \nabla\psi_{\boldsymbol{\xi}} \rangle}{\sqrt{\langle |\nabla\omega|^2 \rangle \langle |\nabla\psi_{\boldsymbol{\xi}}|^2 \rangle}},$$

where $\boldsymbol{\xi} = \nabla^{\perp}\psi_{\boldsymbol{\xi}}$. In Fig.21 we plot them for Case 1 and in Fig.22 for Case 2. Generally speaking, they grow in magnitude with time, except for gradients in Case 1 where a non-monotonic behavior is seen. In Case 1, the vorticity gradient $|\nabla\omega|$ and the Jacobi field $|\nabla\psi_{\boldsymbol{\xi}}|$ are not well correlated at late times. In fact, it is the passive scalar gradient $|\nabla\theta|$ that has a better correlation with the Jacobi field (see Fig.23 below). We study the matrix $\boldsymbol{M}$ described in Section II.B in connection with passive scalar dispersion in this sense. In Fig.23 the time-evolution of contours of passive scalar for Case 1 is given. The initial condition is

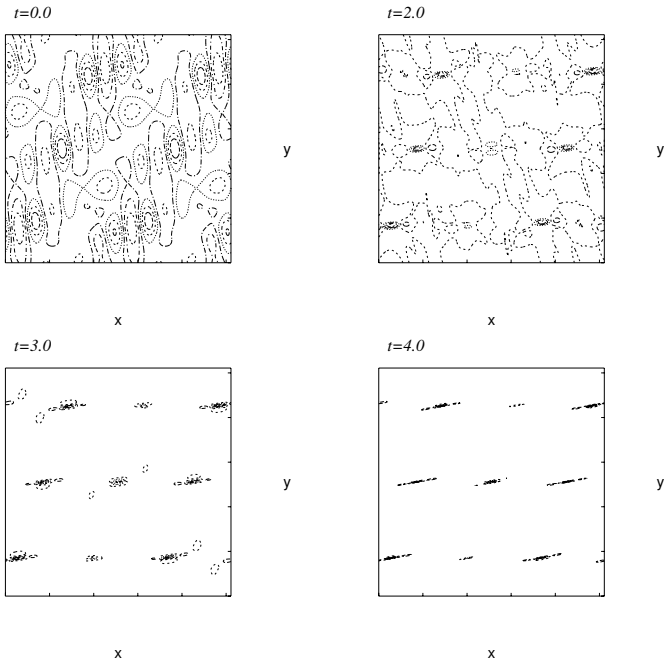

FIG. 14: Time evolution of contours of the integrand of the sectional curvature $\boldsymbol{\xi} \cdot \boldsymbol{P} \cdot \boldsymbol{\xi} - |\nabla \alpha_{\boldsymbol{\xi}}|^2$ for Case 1. Plotted similarly as in Fig.12.

taken as

$$\theta(\boldsymbol{x}) = -\Delta \psi_{\boldsymbol{\xi}}(\boldsymbol{x}).$$

In Fig.24 the corresponding contours for $\mathrm{tr}(\boldsymbol{M})$ are plotted. By comparing them we see that at late times $t = 4.0$ characteristic structures in $\mathrm{tr}(\boldsymbol{M})$ are observed where contours of the passive scalar field is stretched intensely. Recall that these locations coincide with peripheral regions between vortices with steep vorticity gradient (Fig.12). At least qualitatively, the observations support the view that $\boldsymbol{M}$ is related with particle dispersion. It should be noted that the locations are markedly different from those with large negative sectional curvature. To summarize, in Case 1, the Jacobi field, the sectional curvature and scalar gradient are strongly correlated and are mildly correlated with vorticity gradient. The vorticity gradient is well correlated with $\mathrm{tr}(\boldsymbol{M})$ and is mildly correlated with scalar gradient. For Case 2, all the five fields are well correlated in their characteristic structure (figures for θ and $\mathrm{tr}(\boldsymbol{M})$ are omitted).

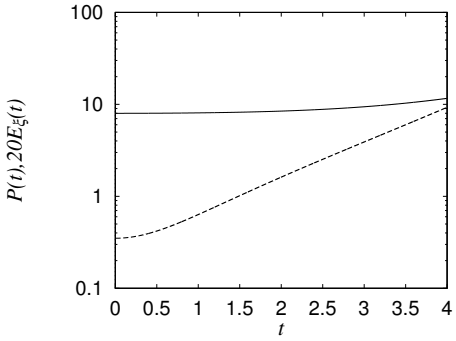

FIG. 15: Time evolution of $P(t) = \frac{1}{2}\left\langle |\nabla\omega|^2 \right\rangle$, (solid) and $20E_{\boldsymbol{\xi}}(t) = 10\left\langle |\boldsymbol{\xi}|^2 \right\rangle$ (dashed) for Case 1.

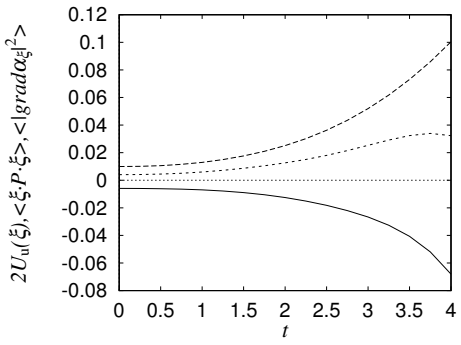

FIG. 16: Time evolution of unnormalized sectional curvature $2U_{\boldsymbol{u}}(\boldsymbol{\xi})$ (solid), $\left\langle |\nabla\alpha_{\boldsymbol{\xi}}|^2 \right\rangle$ (dashed) and $\langle \boldsymbol{\xi}\cdot\boldsymbol{P}\cdot\boldsymbol{\xi}\rangle$ (short-dashed) for Case 1. The dotted line represents 0.

V. SUMMARY AND DISCUSSION

We have discussed Arnold's theory of Euler equations numerically on the basis of Rouchon's formulation. After working out the sectional curvatures analytically for some initial conditions, we have solved numerically the Euler equations and the Jacobi equations simultaneously. The results on the Jacobi field and the sectional curvatures are presented both in two and three dimensions.

A growing correlation of the Jacobi fields with the vorticity is observed in 3D and with the scalar gradient (and with the vorticity gradient in some case) in 2D. Rouchon's integral expression for the sectional curvature is made up of two parts. It is found that $|\nabla\alpha_{\boldsymbol{\xi}}|^2$ grows much faster than $\boldsymbol{\xi}\cdot\boldsymbol{P}\cdot\boldsymbol{\xi}$. In 2D, we observe that even if $K(\boldsymbol{u},\boldsymbol{\xi}) > 0$ at $t = 0$, soon we have $K(\boldsymbol{u},\boldsymbol{\xi}) < 0$. Moreover, the spatial structure of the vorticity and the fields are examined in some details, including the relationship between a passive scalar field and the matrix $\boldsymbol{M}$ is studied.

We have observed exponentially growth in the Jacobi field in most cases. This may not be totally trivial because it was pointed out[10] that the Jacobi field does not always grow exponentially in time even though the corresponding sectional curvature is negative. Indeed, it was shown that it is impossible to have a flow which is stable in the Eulerian sense and is exponentially unstable in the Lagrangian sense[10]. Here, the Eulerian and Lagrangian perturbations are measured by $\boldsymbol{f}$ and $\boldsymbol{\xi}$, respectively. More precisely, if $\boldsymbol{u}$ a steady solution

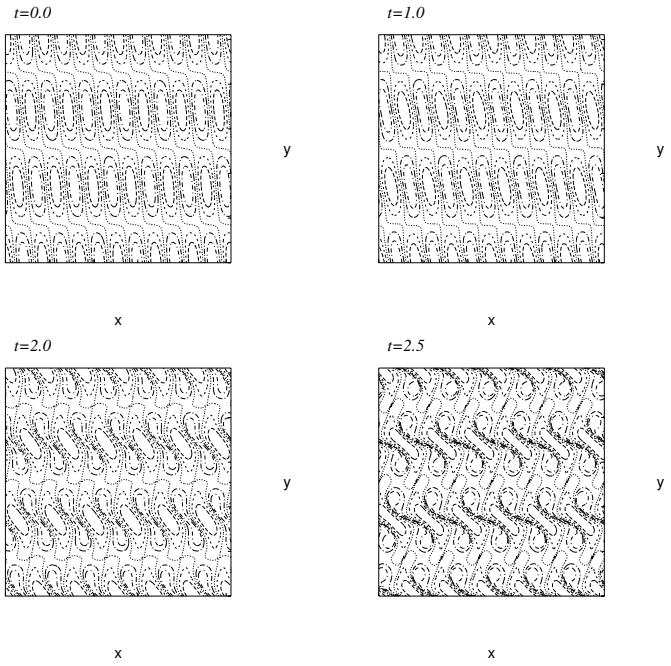

FIG. 17: Time evolution of contours of vorticity ω for Case 2. Plotted similarly as in Fig.12.

of the 2D Euler equations with no stagnation points, then we have

$$\|\boldsymbol{\xi}\|(t) \leq \sqrt{3+2At^2}\frac{\sup_{\boldsymbol{x}}|\boldsymbol{u}|}{\inf_{\boldsymbol{x}}|\boldsymbol{u}|}\int_0^t \|\boldsymbol{f}\|(t')dt',$$

where A is a constant. An example was given therein by using a plane parallel Couette flow, where a negative sectional curvature arises for such a peculiar case, which is stable and has only a continuous spectrum.

A possible singularity formation in inviscid flows is thought to be related to the (physically important) onset of turbulence. The Hamiltonian methods may be useful for studying the blow-up/regularity issues of the 3D Euler equations, while we refrain from discussing such delicate matters because of limited spatial resolutions. Nevertheless, it may be of interest to seek regularity criteria in terms of the geometric quantities, such as the sectional curvature. For example,the well-known Beale-Kato-Majda criterion[27] states that

$$\int_0^T \sup_{\boldsymbol{x}}|\boldsymbol{\omega}(\boldsymbol{x},t)|dt < \infty$$

for the regularity of a 3D Euler flow on a time-interval $[0,T)$. As its variant we can show that if the pressure Hessian is regular then no singularity can form for the Euler flow in a

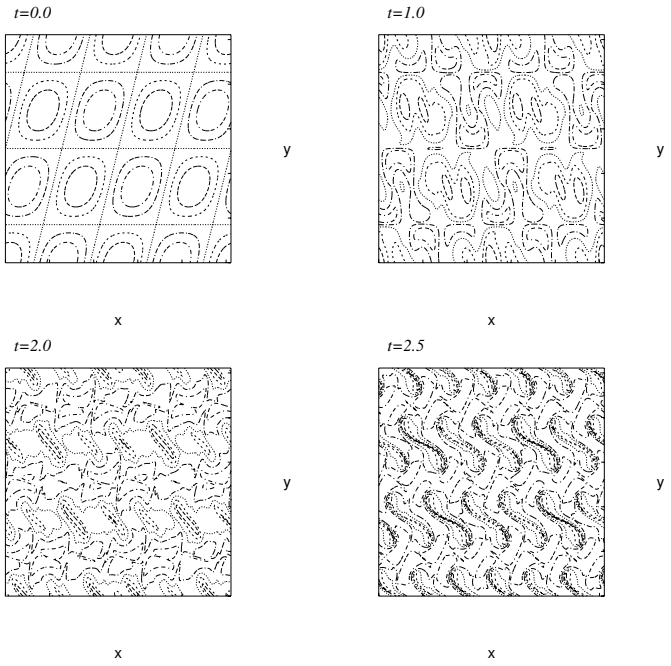

FIG. 18: Time evolution of contours of the Jacobi field $\psi_{\boldsymbol{\xi}}$ for Case 2. Plotted similarly as in Fig.12.

number different of manners[21,27,28]. It is of interest to examine whether or not the curvature can remain bounded, that is,

$$\int \left(\boldsymbol{\xi}\cdot\boldsymbol{P}\cdot\boldsymbol{\xi} - |\nabla\alpha_{\boldsymbol{\xi}}|^2\right) d\boldsymbol{x} < \infty, \quad \text{for any } \boldsymbol{\xi}$$

at a time of possible singularity. Some of the recent works[30–33] on related problems appear to be promising.

Acknowledgments

Part of this work was presented at a seminar at University of Warwick on March 8, 2008. The author thanks R. Kerr and M. Bustamante for some useful comments. This work was presented at an Institute for Mathematics and its Applications (IMA) Conference "Analysis and Computation of Incompressible Fluid Flow" at University of Minnesota, during February 22-26, 2010. He also thanks S.C. Preston and G. Misiolek for useful comments. This work has

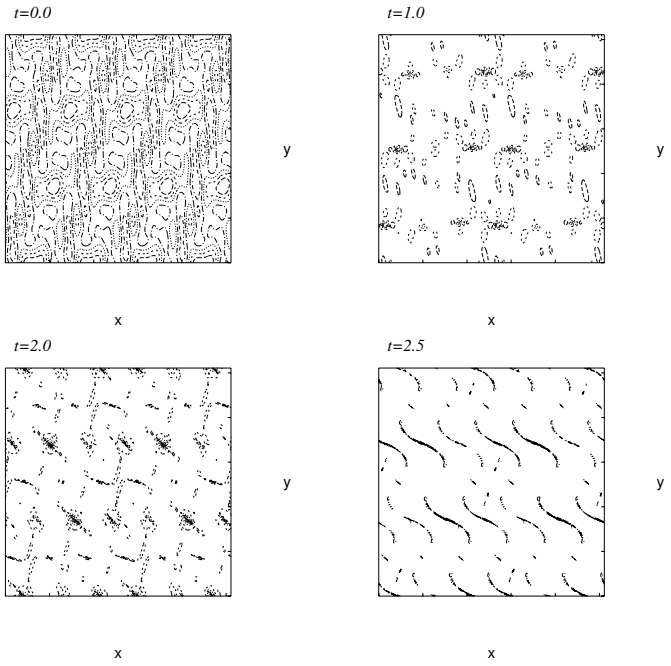

FIG. 19: Time evolution of contours of the integrand of the sectional curvature $\boldsymbol{\xi} \cdot \boldsymbol{P} \cdot \boldsymbol{\xi} - |\nabla \alpha_{\boldsymbol{\xi}}|^2$ for Case 2. Plotted similarly as in Fig.12.

been partially supported by an EPSRC grant EP/F009267/1. He has also been supported by Royal Society Wolfson Research Merit Award.

---

[1] V.I. Arnold, "Sur la geometrie differentielle des groupes de Lie de dimension infinie et ses applications a l'hydrodynamique des fluides parfaits," Annales de l'institut Fourier **16**, 319(1966).

[2] V.I. Arnold, *Mathematical Methods of Classical Mechanics,* (Springer, Berlin, 1978).

[3] V.I. Arnold and B. Khesin, *Topological methods in hydrodynamics,* (Springer, Berlin, 1998.)

[4] F. Nakamura, Y. Hattori and T. Kambe, "Geodesics and curvature of a group of diffeomorphisms and motion of an ideal fluid," J. Phys. A: Math. Gen. **25**, L45(1992).

[5] Y. Hattori, "Ideal magnetohydrodynamics and passive scalar motion as geodesics on semidirect product groups" J. Phys. A: Math. Gen. **27**, L21(1994).

[6] J. Marsden, D.Ebin and A. Fischer, Diffeomorphism groups, hydrodynamics and relativity.

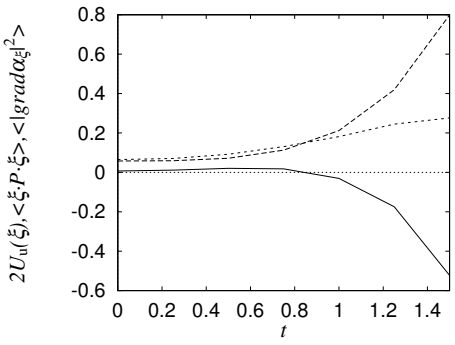

FIG. 20: Close-up of time evolution of unnormalized sectional curvature $2U_{\boldsymbol{u}}(\boldsymbol{\xi})$ (solid), $\left\langle |\nabla \alpha_{\boldsymbol{\xi}}|^2 \right\rangle$ (dashed) and $\langle \boldsymbol{\xi} \cdot \boldsymbol{P} \cdot \boldsymbol{\xi} \rangle$ (dotted) for Case 2. The dotted line represents 0.

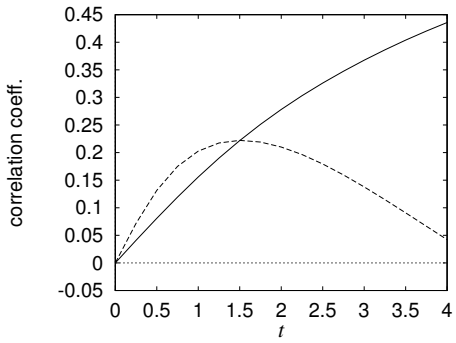

FIG. 21: Time evolution of correlation between the vorticity gradient and the Jacobi field for Case 1: $r(\omega, \psi_{\boldsymbol{\xi}})$ (solid), $r(\nabla\omega, \nabla\psi_{\boldsymbol{\xi}})$ (dashed).

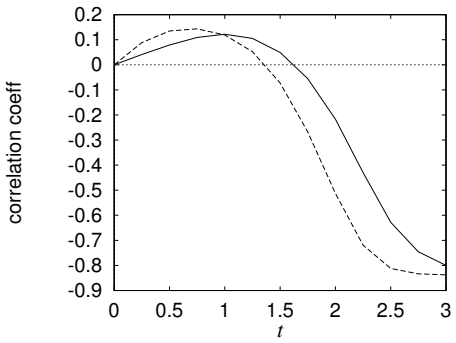

FIG. 22: Time evolution of correlation between the vorticity gradient and the Jacobi field for Case 2: $r(\omega, \psi_{\boldsymbol{\xi}})$ (solid), $r(\nabla\omega, \nabla\psi_{\boldsymbol{\xi}})$ (dashed).

In Proc. 13th Biennial Seminar of Canadian Math. Congress (J. R. Vanstone, ed.), Montreal, 1972, pp. 135-279.

[7] J. Marsden and D. Ebin, "Groups of diffeomorphism and the motion of an incompressible fluid" Ann. of Math, **92**, 102(1970).

[8] G. Misiolek, "Stability of flows of ideal fluids and the geometry of the group of diffeomorphisms," Indiana Univ. Math. J. **42**, 215(1993).

[9] S.C. Preston, "Eulerian and Lagrangian stability of fluid motions," PhD Thesis, SUNY Stony Brook, (2002).

[10] S.C. Preston, "For Ideal Fluids, Eulerian and Lagrangian Instabilities are Equivalent," Geom.

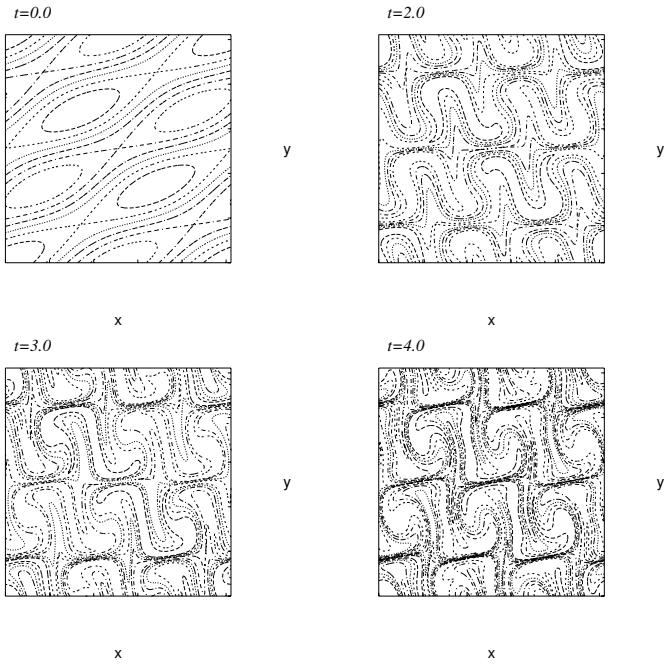

FIG. 23: Time evolution of contours of passive scalar θ for Case 1 in $[0, 2\pi]^2$. Plotted similarly as in Fig.12.

Funct. Anal. **14**, 1044(2004).

[11] P. Rouchon, "Jacobi equation, Riemannian curvature and the motion of a perfect incompressible fluid," Eur. J. Mech. B/Fluids **11**, 317(1992).

[12] P. Rouchon, "Dynamique des fluides parfaits, principe de moindre action, stabilité lagrangienne," Technical Report 13/3446 EN, ONERA (1991).

[13] J.F.C. van Velsen, "Curvature statistics of some few-body Debye-Huckel and Lennard-Jones systems," J. Phys. A: Math. Gen. **13**, 833(1980).

[14] J.F.C. van Velsen, "The average Riemann curvature of conservative systems in classical mechanics," J. Phys. A: Math. Gen. **14**, 1621(1981).

[15] J.F.C. van Velsen, "On the Riemann curvature of conservative systems in classical mechanics," Phys. Lett. **67A**, 325(1978).

[16] T. Kambe, *Geometrical theory of dynamical systems and fluid flows,* (World Scientific, New Jersey, 2004).

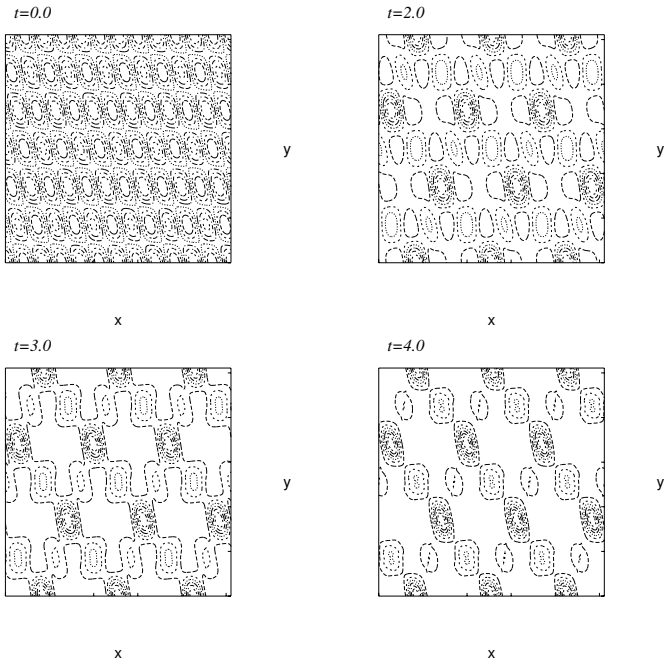

FIG. 24: Time evolution of contours of the trace $\mathbf{tr}(\boldsymbol{M})$ of the matrix $\boldsymbol{M}$ for Case 1 in $[0, 2\pi]^2$. Plotted similarly as in Fig.12.

[17] R. Salmon, *Lectures on geophysical fluid dynamics,* (Oxford University Press, Oxford,1998).

[18] P.J. Morrison, "Hamiltonian description of the ideal fluid" Rev. Mod. Phys.**70**, 467(1998).

[19] P. Ehrenfest "Die bewegung starrer körper in Flüssigkeiten und die Mechanik von Hertz" in *Collected Scientific Papers*, ed. Martin J. Klein, *et al.* (North Holland Publishing: Amsterdam, 1959).

[20] C. Lanczos, *The Variational Principles of Mechanics*, (Dover, New York, 1986).

[21] K. Ohkitani and S. Kishiba, "Nonlocal Nature of Vortex Stretching in an Inviscid Fluid," Phys. Fluids **7**, 411(1995).

[22] J.J. Moreau, "Une methode de 'cinematique fonctionnelle' en hydrodynamique" C.R. Acad. Sci. Paris, **229**, 2156(1959).

[23] The equations (1), (3) and (4) correspond to the geodesic equation $\dfrac{d^2x^i}{dt^2} + \Gamma^i_{jk}\dfrac{dx^j}{dt}\dfrac{dx^k}{dt} = 0$, the geodesic deviation $\dfrac{d^2w^i}{dt^2} = -R^i_{jkl}\dfrac{dx^j}{dt}w^k\dfrac{dx^l}{dt}$, and $\dfrac{d^2}{dt^2}\dfrac{w_iw^i}{2} = \dfrac{dw_i}{dt}\dfrac{dw^i}{dt} - R_{ijlk}w^i\dfrac{dx^j}{dt}w^l\dfrac{dx^k}{dt}$ in finite dimensional dynamics systems[13]. Here w_i denotes the geodesic deviation, Γ^i_{jk} the

Christoffel symbol and R^i_{jkl} the Riemann tensor.

[24] More precisely, the Jacobi field is defined by $\boldsymbol{\xi} = \frac{\partial}{\partial s}\boldsymbol{x}(\boldsymbol{\phi}^{-1}(\boldsymbol{x},t),t;s)\big|_{s=0}$. Here $\boldsymbol{\phi}^{-1}$ is an inverse (pullback) of a flow map $\boldsymbol{\phi}$, such that $\boldsymbol{x} = \boldsymbol{\phi}(\boldsymbol{a},t)$. It is obtained by solving $\frac{d\boldsymbol{\phi}}{dt} = \boldsymbol{u}(\boldsymbol{\phi}(\boldsymbol{a},t),t)$ subject to an initial condition $\boldsymbol{\phi}(\boldsymbol{a},0) = \boldsymbol{a}$.

[25] In fact, components of $\boldsymbol{\xi}$ parallel to $\boldsymbol{u}$ are irrelevant to the dynamics[11] $\frac{\nabla^2}{\partial t^2}\boldsymbol{\xi}^{\|} = 0$ where $\boldsymbol{\xi} = \boldsymbol{\xi}^{\perp} + \boldsymbol{\xi}^{\|}$, $\boldsymbol{\xi}^{\|} = \frac{\langle \boldsymbol{\xi}, \boldsymbol{u}\rangle}{\langle |\boldsymbol{u}|^2\rangle}\boldsymbol{u}$. We can thus write $\frac{1}{V}\frac{\nabla^2}{\partial t^2}\boldsymbol{\xi}^{\perp} = -\frac{\delta U_{\boldsymbol{u}}(\boldsymbol{\xi}^{\perp})}{\delta \boldsymbol{\xi}^{\perp}}$, where $\frac{\delta}{\delta \boldsymbol{\xi}^{\perp}}$ on the RHS denotes a functional derivative.

[26] S. Kida, "Study of complex singularities by filtered spectral method," J. Phys. Soc. Jpn. **55**, 1542(1986).

[27] J.T. Beale, T. Kato and A. Majda, "Remarks on the breakdown of smooth solutions for the 3-D Euler equations," Commun. Math. Phys. **94**, 61(1984).

[28] D. Chae, "On the finite-time singularities of the 3D incompressible euler equations," Commun. Pure Appl. Math. **60** 597(2007).

[29] P. Constantin, "Singular, weak and absent: Solutions of the Euler equations," Phys. D **237** 1926(2008).

[30] S.C. Preston, "Nonpositive curvature on the area-preserving diffeomorphism group," Journal of Geometry and Physics **53**, 226(2005).

[31] D.G. Ebin, G. Misiolek and S.C. Preston, "Singularities of the exponential map on the volume-preserving diffeomorphism group," Geom. Funct. Anal. **16**, 850(2006).

[32] S.C. Preston, "On the volumorphism group, the first conjugate point is always the hardest," Commun. Math. Phys. **267**, 493(2006).

[33] S.C. Preston, "The WKB Method for conjugate points in the volumorphism group," Indiana Univ. Math. J. **57**, 3303(2008).